Modern Physics Letters B, Vol. 23, Nos. 20 & 21 (2009) 2533–2540

World Scientific
www.worldscientific.com

COMPARISON OF SiC AND ZnO FIELD EFFECT TRANSISTORS FOR HIGH POWER APPLICATIONS

H. ARABSHAHI

Department of Physics, Ferdowsi University of Mashhad,
P.O. Box 91775-1436, Mashhad, Iran
arabshahi@um.ac.ir

Received 22 October 2008
Revised 5 February 2009

An ensemble Monte Carlo method is used to compare the potentialities of SiC and ZnO materials for field effect transistors. First, bulk material electron transport properties are compared and then the operation of MESFETs made from them are investigated. The simulated device geometries and doping are matched to the nominal parameters described for the experimental structures as closely as possible. Simulations of SiC MESFETs of lengths 2, 2.6 and 3.2 μm have been carried out and compared these results with those on ZnO MESFETs of the same dimensions. The direct current IV characteristics of the two materials were found to be similar, though the ZnO characteristics were on the whole superior, reaching their operating point at higher drain voltages and possessing higher gains. However, oscillations in the drain current caused by changes in drain voltage in the ZnO devices were not present to the same degree in the SiC devices. This difference is caused partially by the onset of the negative differential regime in SiC at a higher electric field than in ZnO but the primary cause is the longer ballistic transport times in SiC. This suggests that ZnO MESFETs may prove to have superior frequency response characteristics than SiC MESFETs.

Keywords: Drain current; gain, negative differential; frequency response.

1. Introduction

In recent years, there has been an increasing interest in using the wide band gap semiconductors SiC and ZnO for microwave power amplification. Monte Carlo simulations predict a peak electron velocity of 2.2×10^5 ms^{-1} and 2.5×10^5 ms^{-1} for SiC and ZnO materials, respectively.[1–5] This makes high frequency operation devices possible.

The metal semiconductor field effect transistor (MESFET) is one of the most favored devices in the construction of large scale integrated circuits because of its simplicity of construction, the comparative lack of dopant diffusion problems and the resultant high packing densities. Whilst the preferred semiconductor is still silicon, industry is now tooling up for wide band gap semiconductors like SiC or ZnO production, which offers high electron mobility and hence the prospect of greater frequency operating rates. Their direct band gap furthermore allows

easier integration with optical devices. For this reason SiC MESFETs have received much attention in the literature, particularly with respect to their simulation[6,7] in an attempt to understand the basic principles of their operation. Monte Carlo methods have been used to a great extent in this effort because they allow an essentially exact solution of the Boltzmann transport equation and are subject only to statistical errors, unlike drift diffusion models which cannot accurately treat the hot-electron effects that are present to a high degree in SiC devices.[8] ZnO offers the prospect of mobilities comparable to SiC and is increasingly being developed for the construction of optical switches. Other authors have also pointed out the potential importance of ZnO and a few simple devices have been simulated.[9] This paper presents the results of a Monte Carlo simulation which is used to model electron transport in wurtzite SiC and ZnO MESFETs including different tansistor lengths at room temperature. The simulations have been carried out using a non-parabolic ellipsoidal valley model to describe transport in the conduction band.

This article is organized as follows. Details of the device fabrication model which is used in the simulated device are presented in Sec. 2, and results for simulation carried out on SiC and ZnO MESFETs are interpreted in Sec. 3.

2. Model Details

The Monte Carlo method may be used to simulate the motion of charge carriers through a semiconductor device by following the progress of several tens of thousands of test or representative superparticles. These particles are propagated classically between collisions according to their velocity, effective mass and the prevailing field. The selection of quantities such as the propagation time of a particle between scattering events or the mechanism by which the particle is to be scattered is done by generating a random number and using the number to choose the required quantity from predetermined tables of probabilities for each process. Thorough discussions of the Monte Carlo method are given by Fawcett *et al.*[10] and Jacoboni *et al.*,[11] and for a review see Moglestue *et al.*[12]

In this work, the two lowest energy conduction bands of the empirical pseudopotential band structure for wurtzite phase of SiC and ZnO are chosen as a basis of an analytical multivalley conduction band model.[13–16] The pseudopotential band structure shows the conduction band minimum to be located at the Γ point (Γ_1), and lowest energy conduction band satellite valleys to occur at the U point (located about two thirds of the way between the L and M symmetry points). Higher conduction band valleys are located at the Γ point (Γ_3), at the M point, and at the K point. In our Monte Carlo simulation, the two different Γ valleys, the six equivalent U valleys, the three equivalent M valleys, and the two equivalent K valleys, are represented by ellipsoidal, non-parabolic dispersion relationships of the following form[11,12]

$$E(\mathbf{k})[1+\alpha_i E(\mathbf{k})] = \frac{\hbar^2}{2}\left[\frac{k_x^2+k_y^2}{m_\perp^*}+\frac{k_z^2}{m_\parallel^*}\right], \tag{1}$$

Table 1. Important parameters used in our simulations for wurtzite phase SiC and ZnO.

Bulk material parameters	SiC	ZnO			
Density ρ (kgm^{-3})	3200	5600			
Longitudinal sound velocity v_s (ms^{-1})	1373	6400			
Low-frequency dielectric constant ϵ_s	9.7	8.2			
High-frequency dielectric constant ϵ_∞	6.5	3.7			
Acoustic deformation potential D (eV)	15	14			
Polar optical phonon energy $\hbar\omega_{op}$ (meV)	120	72			
Band Gap E_g (meV)	3.2	3.43			
Valley dependent parameters	Γ_1	U	Γ_3	M	K
Effective mass (m^*/m_0):					
SiC	0.28	0.39	0.6	0.57	0.54
ZnO	0.25	0.4	0.58	0.57	0.3
Nonparabolicity (eV^{-1}):					
SiC	0.32	0.5	0.029	0.0	0.03
ZnO	0.312	0.059	0.02	0.0	0.65
Valley separation from Γ_1-valley (eV):					
SiC	0.0	0.61	1.3	0.9	0.67
ZnO	0.0	2.1	1.8	2.7	2.9
Number of equvalet valley	1	6	1	3	2

where $m^*_\perp$ and $m^*_\parallel$ are the transverse and longitudinal effective masses at the band edge and α_i is the non-parabolicity coefficient of the ith valley. The material and valley parameters necessary for calculating the scattering probabilities used in the present Monte Carlo simulation are listed in Table 1.

Electron particles in the employed ensemble Monte Carlo simulation occupy non-parabolic ellipsoidal valleys in reciprocal space, and obey Boltzmann statistics. Herring–Vogt transformations are used to map carrier momenta into spherical valleys when particles are drifted, scattered or cross heterojunctions (where care has been taken to ensure that the crystal momentum in the plane of the junction is conserved across the interface). The electric field equations are solved self-consistently with the electron transport using a finite difference method,[17] and the device grid potentials are updated at each ensemble drift timestep (1 femtosecond). Electrons in the bulk are scattered by ionized impurities and by bulk acoustic and non-polar optical phonon modes. Intervalley scattering by the absorption and emission of long wavelength acoustic and optic phonons have also been considered in the model. As described in detail,[11,12] model devices are built up as a series of joined rectangular regions, with the electric field cell sizes matched along the join between each region. Each region can consist of multiple layers of different alloy composition and doping/compensation density.

The SiC/ZnO MESFET can be described simply by three regions (Fig. 1), representing source and drain doping implants and a central region containing the supply layers. The field cell size used for the central region is 30 nm^2 (horizontal $\times$

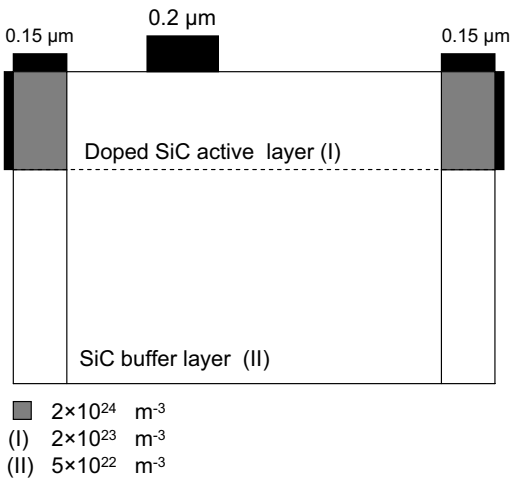

Fig. 1. The two-dimensional model of SiC/ZnO MESFET. The modeled structure is divided into three regions, as indicated. Electron particles are initially distributed keeping all regions charge-neutral. The location of the source and the drain implants and the top and back buffer layer are marked.

vertical), but that in the high doped source and drain implants is finer (10 nm^2). Simulations of steady current characteristics have been carried out using 20000 electron paticles.

Figure 1 shows a schematic of the modeled SiC/ZnO MESFET. The overall device length is 2 μm in the x-direction and the device has a 0.2 μm gate length and 0.15 μm source and drain length. The source and drain have ohmic contacts and gate is in Schottky contact in 1 eV to represent the contact potential at Au/Pt. The source and drain regions are doped to 2×10^{24} m^{-3} electron concentration and the top and down buffer layers are doped to 2×10^{23} m^{-3} and 5×10^{22} m^{-3} electron concentration, respectively.

The drain current is obtained by counting the net charge flow through the drain contact. For the static IV characteristics, the simulation was continued until the current converged to a value with an error of less than 1 Å in two successive 10 ps intervals.

The relationships between field and drift velocity obtained for each material are shown in Fig. 2, where they are seen to compare well with Refs. 18–20.

3. Results and Discussion

The computed $I_{ds}(V_{ds}, V_{gs})$ characteristics are presented in Fig. 3 for both SiC and ZnO MESFET. The obtained characteristics are almost identical in shape. For both structures, one observes that the output conductance is quite large and that the device is not completely pinched-off even at large negative gate bias. These two effects are mainly due to short channel effects and strong electron injection in

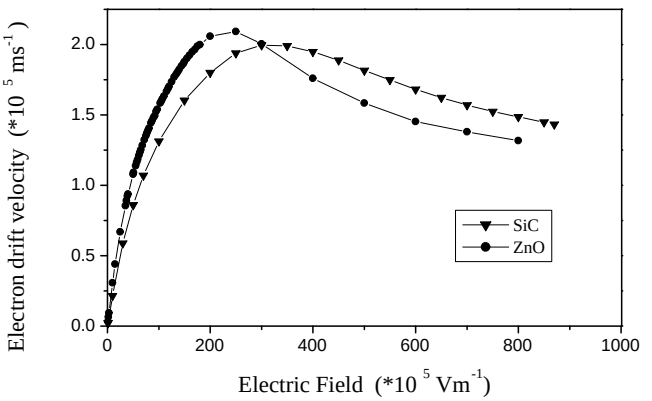

Fig. 2. Relationships between electron drift velocity and electric field for ZnO (circles) and SiC (triangles) found using the parameters of Table 1.

the buffer layer. A part of the drain current flows through the buffer and increases with increasing drain voltage. This effect is more important at high V_{gs}, e.g. at $V_{gs} = -13$ V, the whole drain current flows entirely through the buffer. This is due to the low conduction band discontinuity at the interface between SiC/ZnO and their buffer layers. Nevertheless, for both structures, high drain current densities are obtained, confirming that SiC or ZnO MESFETs are good candidates for high power applications. Moreover, due to the better electronic transport properties in ZnO, the ZnO based MESFET exhibits a 55% higher drain current density as compared with the SiC MESFET.

The effect of device length on output drain current have also been studied in Fig. 3. It is apparent from this figure, that higher drain current are reached as the device length is reduced as a result of the increase in longitudinal electric field and velocity overshoot effects. It follows that the electron transit time under the gate is reduced in two ways. There is a reduction in the transit length and also the electron velocity is larger. The high value of the field at the source-end of the gate is responsible for the almost ballistic acceleration of the electrons as soon as they enter the channel region under the gate. As a result, shorter devices lead to higher cut-off frequencies but they are also expected to lead to smaller breakdown voltages.

Figures 4 and 5 present the evolution of transconductance g_m (Fig. 4) and current gain cut-off frequency f_c (Fig. 5) versus gate voltage V_{gs}, at $V_{ds} = 30$ V, for both structures. Due to the better electronic properties and higher drain current densities, ZnO MESFET exhibits 55% higher transconductance and cut-off frequency. For example, at $V_{gs} = 0.2$ V, we obtained transconductance of 260 mS mm^{-1} and cutoff frequency of 100 GHz for the ZnO MESFET, against 160 mS mm^{-1} and 85 GHz for the SiC. These results show that ZnO MESFETs may perform quite well for high frequency operations as well as for high power applications.

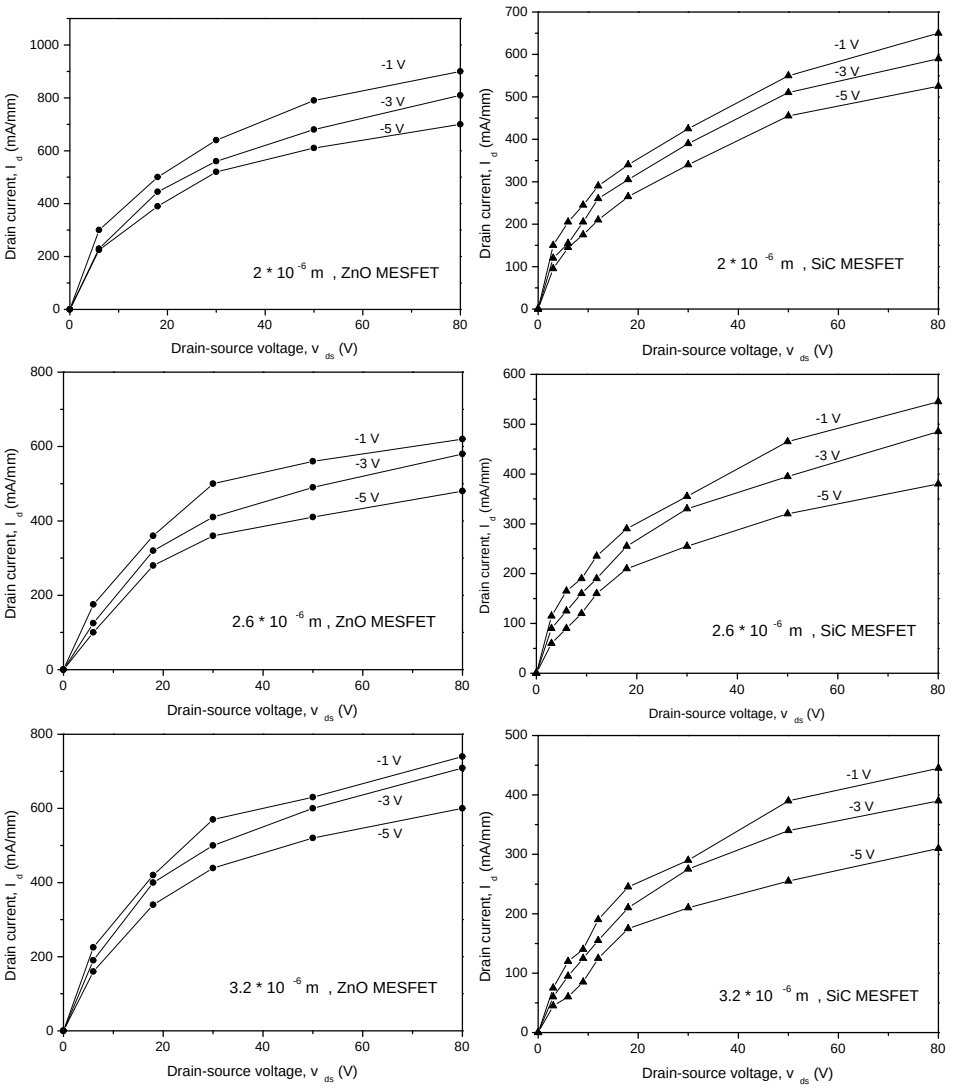

Fig. 3. Static IV characteristics for ZnO and SiC MESFETs for effective gate voltages of -1 V to -5 V and for different device length.

4. Conclusion

The Monte Carlo technique has been used to compare the potentialities of ZnO and SiC MESFETs. We find that both materials are good candidates for high frequency and high power operations. At low operation frequencies, ZnO drain IV characteristics are superior to those of SiC, possessing greater output resistances and higher gains. However, the SiC devices displayed substantially greater stability

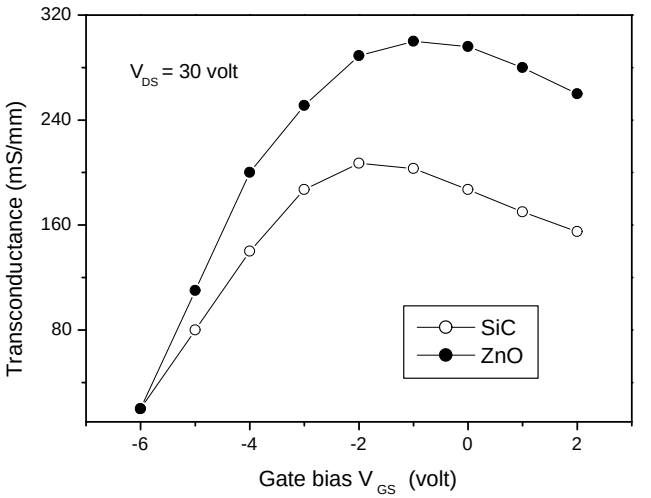

Fig. 4. Transconductance as a function of gate bias. Comparison of ZnO and SiC MESFET.

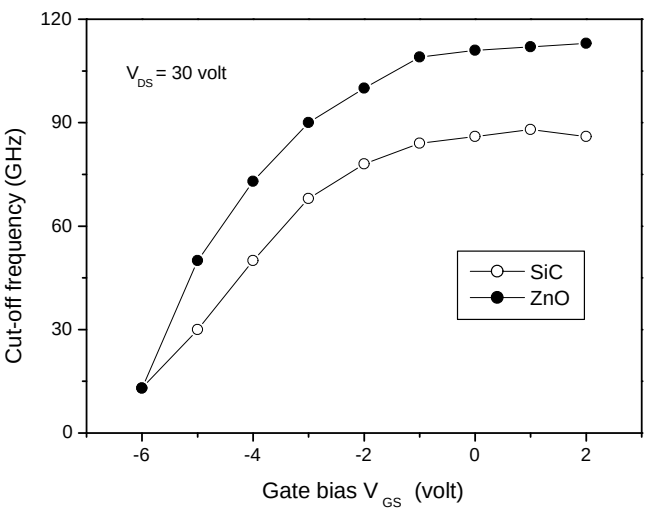

Fig. 5. Current gain cut-off frequency as a function of gate bias. Comparison of ZnO and SiC MESFET.

with respect to changes of voltage because of the ability of SiC to maintain a positive differential resistance at the drain contact due to ballistic effects under the gate.

Acknowledgment

The author wishes to thank M. G. Paeezi for helpful comments and for critical reading of the manuscript.

References

1. R. Mickevicius and J. H. Zhao, *J. Appl. Phys.* **83** (1998) 3161.
2. D. C. Look, D. C. Reynolds, J. R. Sizelove and W. C. Harsch, *Solid State Commun.* **105** (1998) 399.
3. D. C. Look, *Mater. Sci. Eng. B*, **80** (2001) 383.
4. J. D. Albrecht, P. P. Ruden, S. Limpijumnong and K. F. Brennan, *J. Appl. Phys.* **86** (1999) 6864.
5. T. Makino, Y. Segawa, A. Tsukazaki, A. Ohtomo and M. KaWasaki, *Appl. Phys. Lett.* **87** (2005) 022101.
6. K. Dohnke, R. Rupp, D. Peters, J. Volkl and D. Stephani, *Institute of Physics Conf. Series* (IOP Publishing, Bristol, UK, 1994), p. 625.
7. A. K. Agarwal, *The Second Int. Electric Electronic Combat Vehicle Conf. AECV-II* (Dearborn, MI, 1997).
8. R. P. Joshi, *J. Appl. Phys.* **78** (1995) 5518.
9. H. E. Nilsson, U. Sannemo and C. S. Petersson, *J. Appl. Phys.* **80** (1996) 3365.
10. W. Fawcett, A. D. Boardman and S. J. Swain, *J. Phys. Chem. Solids* **31** (1963).
11. C. Jacoboni and P. Lugli, *The Monte Carlo Method for Semiconductor and Device Simulation* (Springer-Verlag, 1989).
12. C. Moglestue, *Monte Carlo Simulation of Semiconductor Devices* (Chapman and Hall, 1993).
13. H. Arabshahi, *Mod. Phys. Lett. B* **20** (2006) 787.
14. H. Arabshahi and M. H. Ghasemian, *Mod. Phys. Lett. B* **22** (2006) 1397.
15. H. Arabshahi, M. R. Benam and B. Salahi, *Mod. Phys. Lett. B* **21** (2007) 1715.
16. H. Arabshahi, *Mod. Phys. Lett. B* **21** (2007) 199.
17. M. Walmsley and R. A. Abram, *Comput. Math. Electr. Electron. Eng.* **15** (1996) 31.
18. J. B. Roldan, F. Gamiz, J. A. Lopez-Villanueva and P. Cartujo, *J. Electron Matter* **26** (1997) 203.
19. R. Mickevicius and J. H. Zhao, *J. Appl. Phys.* **83** (1998) 3161.
20. Y. C. Yeo, T. C. Chong and M. F. Li, *J. Appl. Phys.* **83** (1998) 1429.